Hindawi
Shock and Vibration
Volume 2023, Article ID 2530651, 18 pages
https://doi.org/10.1155/2023/2530651

Research Article

Research on Vibration Fatigue Damage Locations of Offshore Oil and Gas Pipelines Based on the GA-Improved BP Neural Network

Yaoguo Xie,[1] **Chengang Gao**,[1] **Puzhe Wang**,[1] **Lei Zhou**,[2] **Chuanjie Zhang**,[2] **and Xianqiang Qu**[1]

[1]*College of Shipbuilding Engineering, Harbin Engineering University, Harbin 150001, China*
[2]*Offshore Oil Engineering Co. Ltd., Tianjin, China*

Correspondence should be addressed to Yaoguo Xie; yaoguoxie@126.com

Received 10 October 2022; Revised 14 February 2023; Accepted 7 March 2023; Published 15 March 2023

Academic Editor: Guangjian Dong

To study vibration fatigue damage localization of offshore oil and gas pipelines, aiming at the location error caused by uncertainty of the initial parameters in backpropagation (BP) neural network training, an improved BP neural network based on the genetic algorithm (GA) is proposed to locate pipeline damage. This approach was verified by experiments and simulations. First, a BP neural network for structural damage location was constructed, and a method to optimize the BP neural network parameters based on the GA was established. Then, a finite element model was established based on the measured data from modal tests of a physical pipeline model, and a large number of vibration neural network training samples were obtained using the finite element model. Finally, to show that the improved BP neural network based on the GA had a better damage location accuracy, the location results of the original BP and GA BP methods were compared for cases with no noise and with 5% noise. The results show that the average error of the BP neural network based on the GA was less than 3%, which was 11.6% lower than that of the original BP neural network.

1. Introduction

Offshore oil and gas production platforms need to be in service for long periods. Once stress beyond a critical level accumulates for a long period, it will induce the initiation of pipeline fatigue cracks, as shown in Figure 1 [1]. Therefore, it is very necessary to conduct damage detection on offshore platform pipelines.

The design of traditional pipelines is based on static analysis, and the vibration of pipelines is rarely considered. Long-term vibration will cause the risk of vibration fatigue damage. For the structure of offshore platform oil and gas pipeline systems in a real environment, the structure of pipeline systems is huge, the pipeline direction is complex, the working environment is complex, and damage detection often needs to be carried out in the working state. Therefore, this paper carries out research on vibration fatigue damage identification of process pipelines and takes vibration-based damage identification as the main route.

For vibration-based damage identification, some scholars have carried out related research and proposed the application scheme. Contursi et al. [2] proposed a new method for locating multiple damaged areas in elastic structures. With truss structures as an example, the locations and degrees of multiple damaged areas could still be correctly predicted when the structural damage level was low. In addition, some scholars proposed a damage prediction method based on the "natural frequency change square ratio," which achieved better results than using the frequency alone. Guo et al. [3] used a BP neural network combined with a modulated broadband mode decomposition (MBMD) method to monitor crane-bearing parts and concluded that the BP neural network has good performance in feature extraction and fault recognition. Rastin et al. [4] presented a novel two-stage technique based on generative

adversarial networks (GANs) for unsupervised structural health monitoring and damage identification. Existing methods to detect structural damage based on the change in structural natural frequency show certain reliability in predicting the location and degree of multiple damage [5–7]. The change in the natural frequency is a function of the damage degree and location of the structure. Some researchers have used this method to identify the damaged structure, and the identification results are very intuitive [8, 9]. However, the problem with this method was that different inducements may lead to the same frequency change, which will be difficult to identify, and this approach is not sensitive enough in the case of small stiffness damage [10]. Others have used neural networks for control and recognition. Tian et al. [11] proposed an improved genetic algorithm (IGA) combined with the global optimization characteristics of the genetic algorithm (GA) and the local optimal solution of the simulated annealing (SA) algorithm in this paper, which adopts SA in the process of selecting subpopulations. Some scholars have found that the neural network has good performance in feature extraction and damage recognition [12, 13].

The main content of this paper is summarized as follows: Section 2 introduces the principle of damage location of BP neural networks. In cases where the training sample size is low, slow learning speeds and convergence to local optimal solutions can occur [14]. In order to improve this problem, this paper proposes an offshore platform pipeline damage location method based on the GA-improved BP neural network. Section 3 explains the design and data source of the experiment. Section 4 is a comparative analysis of the results. Through the analysis of the positioning results of two kinds of neural networks, it is found that the GA-improved BP neural network can effectively improve the positioning accuracy and reduce the average positioning error.

2. Principle of Damage Localization Based on BP and GA BP Neural Networks

2.1. Basic Principle of Structural Damage Identification Based on Modal Parameters. The equation of structural motion in the finite element method is

$$[M]\left\{x''\right\} + [C]\left\{x'\right\} + [K]\{x\} = \{f(t)\}, \tag{1}$$

where $[M]$, $[C]$, $[K]$ represent the discrete mass, damping, and stiffness matrices, respectively, $\left\{x''\right\}$, $\left\{x'\right\}$, $\{x\}$ represent the acceleration, velocity, and displacement vectors, respectively, and $\{f(t)\}$ represents the external load vector. If the damping term is ignored, then

$$[M]\left\{x''\right\} + [K]\{x\} = 0. \tag{2}$$

The solution of this equation is

$$\{x\} = \{\phi\}_i \sin \omega_i t, \tag{3}$$

where ω_i is the ith-order eigenvalue and $\{\phi\}_i$ is the corresponding eigenvector of the ith-order eigenvalue. The relation between $[M]$, $[K]$ and $\omega_i, \{\phi\}_i$ can be obtained by substituting equations (3) into (2) as follows:

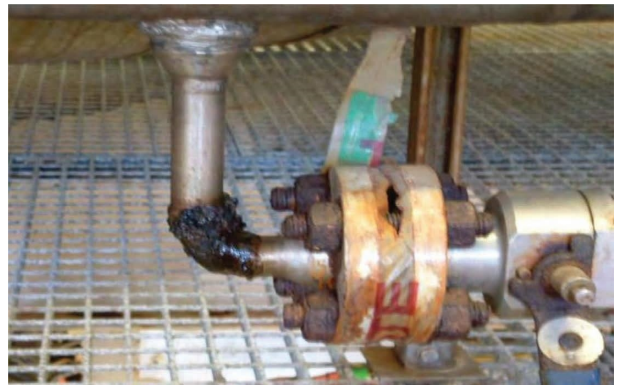

Figure 1: Example of pipeline fatigue cracks.

$$[K]\{\phi\}_i - \omega_i^2 [M]\{\phi\}_i = 0. \tag{4}$$

We can see that $\omega_i, \{\phi\}_i$ are functions of $[M]$, $[K]$ of the structure. Any change in $[M]$, $[K]$ of the structure will be reflected in the measured value of $\omega_i, \{\phi\}_i$. When the measured modal parameters of the structure are significantly different from those of the reference model (beyond the measured error range), it can be judged that the structure has been damaged. Therefore, the structural damage can be determined by comparing the modal parameters before and after the structural damage [15].

2.2. Backpropagation (BP) Neural Network

2.2.1. Overview of the BP Neural Network. The BP neural network is the most widely used neural network structure at present, and it is composed of an input layer, hidden layer, and output layer. It can realize complex mappings from an input to an output [16]. BP is error backpropagation. It adjusts the weights and thresholds between neurons at each layer through the error of the actual output compared with the expected output such that the output of the neural network is constantly approaching the expected output.

Its basic structure is shown in Figure 2. The number of nodes in the network input layer, hidden layer, and output layer is m, h, and n, respectively. $x = (x_1, \ldots, x_m)^T$ is the input training sample, $y = (y_1, \ldots, y_h)^T$ is the hidden layer output, and $z = (z_1, \ldots, z_n)^T$ is the network output. Signal forward propagation and error backpropagation are repeated until the training error is small enough, and neural network training is completed.

2.2.2. Structural Damage Location Method Based on the BP Neural Network. The selection of the input and output vectors in the BP neural network has a significant influence on network performance. For offshore oil and gas pipelines, it is difficult to obtain accurate modal information in the complex environment. The natural frequency and structure are relatively easy to obtain. Furthermore, based on previous research, the change in the natural frequency and the structural damage location are correlated [17].

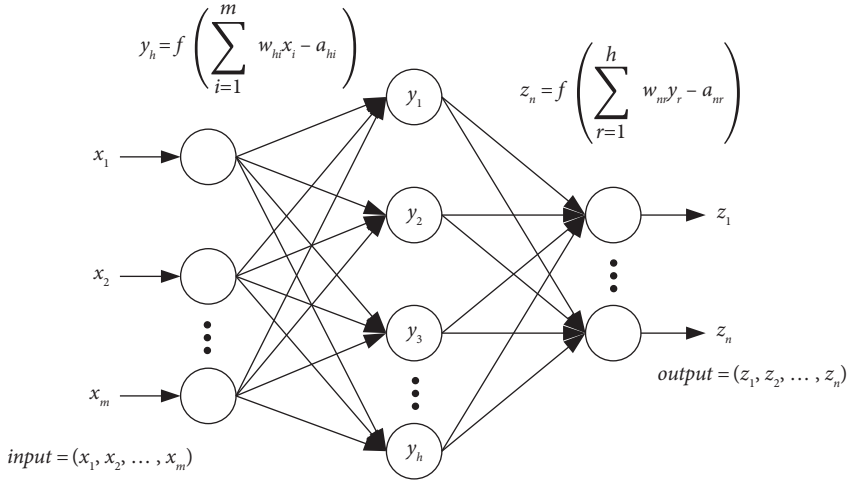

Figure 2: Structure of the backpropagation (BP) neural network.

The change rate of the structure's natural frequency of the order, i, is

$$\mathrm{FFC}_i = \frac{\omega_i - \omega_j}{\omega_i}, \tag{5}$$

where ω_i is the natural frequency of the nondestructive structure and ω_j is the natural frequency of the structure after damage. By introducing equations (4) and (5), we obtain

$$\mathrm{FFC}_i = g_i(r) f_i(\Delta K, \Delta M), \tag{6}$$

where r is the vector of the structural damage position and FFC_i is related to the damage degree and damage location of the structure.

The Taylor expansion of f_i about $\Delta K = 0$ and $\Delta M = 0$, ignoring higher order terms, can be obtained as follows:

$$\mathrm{FFC}_i = g_i(r) \times \left[f_i(0,0) + \Delta M \frac{\partial f_i}{\partial \Delta M}(0,0) + \Delta K \frac{\partial f_i}{\partial \Delta K}(0,0) \right]. \tag{7}$$

Since $f_i(0,0) = 0$ in this formula,

$$\mathrm{FFC}_i = g_i(r) \times \left[\Delta M \frac{\partial f_i}{\partial \Delta M}(0,0) + \Delta K \frac{\partial f_i}{\partial \Delta K}(0,0) \right]. \tag{8}$$

The partial derivatives of the function, f_i, at $\Delta K = 0$ and $\Delta M = 0$ is constant, so

$$\mathrm{FFC}_i = \Delta M m_i(r) + \Delta K n_i(r). \tag{9}$$

In general, structural damage is mainly the change in structural stiffness, so by assuming $\Delta M = 0$, the following can be obtained:

$$\mathrm{FFC}_i = \Delta K n_i(r). \tag{10}$$

The normalized frequency change rate is

$$\mathrm{NFCR}_i = \frac{\mathrm{FFC}_i}{\sum_{i=1}^{m} \mathrm{FFC}_m} = \frac{\Delta K n_i(r)}{\Delta K \sum_{i=1}^{m} n_m(r)} = l_i(r), \tag{11}$$

where m is the frequency order considered in the analysis.

It can be found that NFCR is only related to the damage position of the structure, so the neural network input vector is constructed as follows:

$$\{\mathrm{input}\} = \{\mathrm{NFCR}_1, \mathrm{NFCR}_2, \ldots, \mathrm{NFCR}_i, \ldots, \mathrm{NFCR}_m\}. \tag{12}$$

The network output vector is the damage position, and the structure damage location process based on the BP neural network is shown in Figure 3.

2.3. Genetic Algorithm (GA)-Improved BP Neural Network Method. The GA is a computational model that simulates natural selection and the genetic mechanism in biological evolution, and it searches for optimal solutions randomly in parallel. The repeated cyclic iteration of the parameters is performed until individuals emerge, which meet the specified requirements [18]. The main advantages of the GA are as follows: The GA has a large search coverage and high efficiency. It can also avoid the problem of falling into the local optimal solutions in the iterative search of a single solution to a certain extent, which is conducive to global optimization. At the same time, selection, crossover, mutation, and other operations in the genetic algorithm have certain randomness, and the search process is more flexible.

The basic idea of using the GA to improve the BP neural network is to search for the optimal initial weights and initial thresholds of the BP neural network through the GA, and the BP neural network with optimized initial parameters can make better predictions [19]. The process is divided into three parts: the determination of the basic structure of the BP neural network, the optimization of the BP neural network parameters by the GA, and the prediction of the optimized BP neural network model, as shown in Figure 4.

The specific process details of the GA-BP approach used in this study are as follows.

2.3.1. Encoding Mode. Real number encoding is adopted. Individual encoding is a real number string composed of all the weights and thresholds of the network. The advantage is

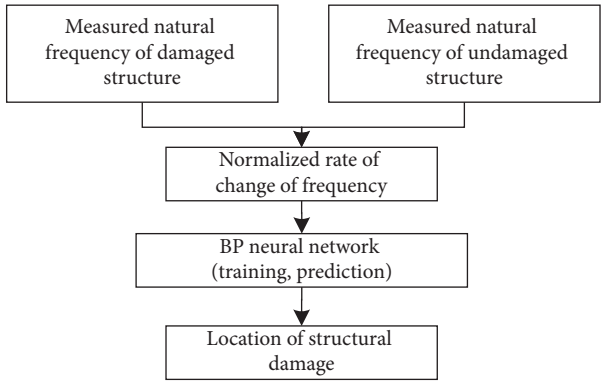

Figure 3: Structural damage location flowchart.

that the encoding mode is simple and that no encoding or decoding operation is needed.

2.3.2. Fitness Function. The weight and threshold information about the neural network contained in the individual is passed to the network structure, and then, the BP neural network is trained with the training data for prediction. The sum of the absolute values of the error between the neural network output and the expected output is taken as the individual's fitness, f, which can be calculated as follows:

$$f = \sum_{i=1}^{n} abs(y_i - o_i), \tag{13}$$

where n is the number of nodes in the output layer of the neural network, y_i is the expected output of the ith node of the neural network, and o_i is the actual output of the ith node of the neural network.

2.3.3. Initialization Process. After the network structure is determined, the coding length is also determined, and a random number in the range of $[-3, 3]$ is selected as the coding of the initial individual to initialize and generate individuals with a specified population size.

2.3.4. Selection Method. The roulette method is adopted; that is, the probability of being selected is allocated according to the fitness value. The selection probability, p_i, of each individual i is

$$p_i = \frac{1/f_i}{\sum_{j=1}^{N}(1/f_i)}, \tag{14}$$

where f_i is the fitness value of the individual, i, which is the sum of the errors, and N is the number of individuals in the population. Based on this equation, the smaller the fitness, the higher the probability of being selected.

2.3.5. Crossover Mode. As individuals are encoded by real numbers, the real number crossing method is adopted to select random locations for single-point crossings. The crossing operation of the kth chromosome a_k and lth chromosome a_l at position j is as follows:

$$\left.\begin{aligned} a_{kj} &= a_{kj}(1-b) + a_{lj}b \\ a_{lj} &= a_{lj}(1-b) + a_{kj}b \end{aligned}\right\}, \tag{15}$$

where b is a random number in the range of $[0, 1]$.

2.3.6. Variation Mode. Mutation occurs randomly with a mutation probability, and basic bit mutation is adopted. The mutation location is randomly selected for the mutation operation in the coding string of the mutation individual, and the jth gene a_{ij} of the ith individual is selected as follows:

$$a_{ij} = \begin{cases} a_{ij} + \left(a_{ij} - a_{\max}\right) * f(g), r > 0.5, \\ a_{ij} + \left(a_{\min} - a_{ij}\right) * f(g), r \le 0.5, \end{cases} \tag{16}$$
$$f(g) = r_2\left(\frac{1-g}{G_{\max}}\right)^2,$$

where $a_{\max}$ is the upper limit of the gene, a_{ij}, $a_{\min}$ is the lower limit of the gene, a_{ij}, g is the current iteration number, $G_{\max}$ is the maximum evolution number, and r, r_2 are the random numbers in the range of $[0, 1]$.

2.3.7. Termination Conditions. Eventually, the average error no longer significantly decreases, or it reaches the upper limit of the number of iterations. At this point, the initial network parameters decoded by the optimal individual are sufficiently close to the optimal initial parameters. On this basis, the neural network is trained to predict damage locations.

3. Pipeline Model Test and Data Processing

3.1. Test Model

3.1.1. Real-Scale Piping System Structure Model. Because the simplified model has some defects, it is difficult to reflect the true situation, so the pipeline adopts the real-scale model. The test model included 4–20 inches of pipes commonly used on offshore platforms, which were made of seamless steel pipes for conveying high-pressure fluid, as stipulated in GB/T 8163-2008 [20]. After consulting relevant pipeline vibration fatigue data [1], three views of the design pipeline are shown in Figures 5(a)–5(c).

3.1.2. Real-Scale Pipe Prefabrication Crack. Because it is very difficult to carry out a fatigue test on real-scale pipelines under laboratory conditions, prefabricated cracks are selected at key locations where fatigue cracks will occur. The purpose of the test is to obtain the modal shapes of the pipeline before and after damage under different damage conditions.

The accuracy of damage locations is the key problem in this paper. The crack is made by cutting the pipeline. In

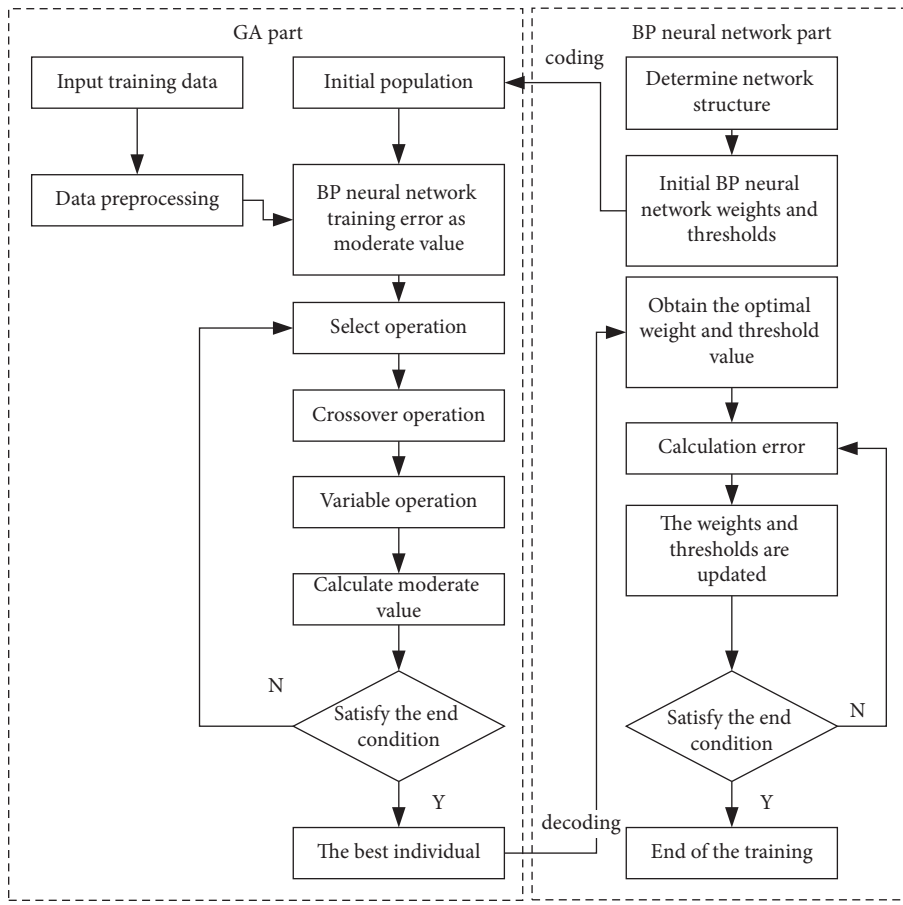

Figure 4: Optimization of the BP neural network by the genetic algorithm (GA).

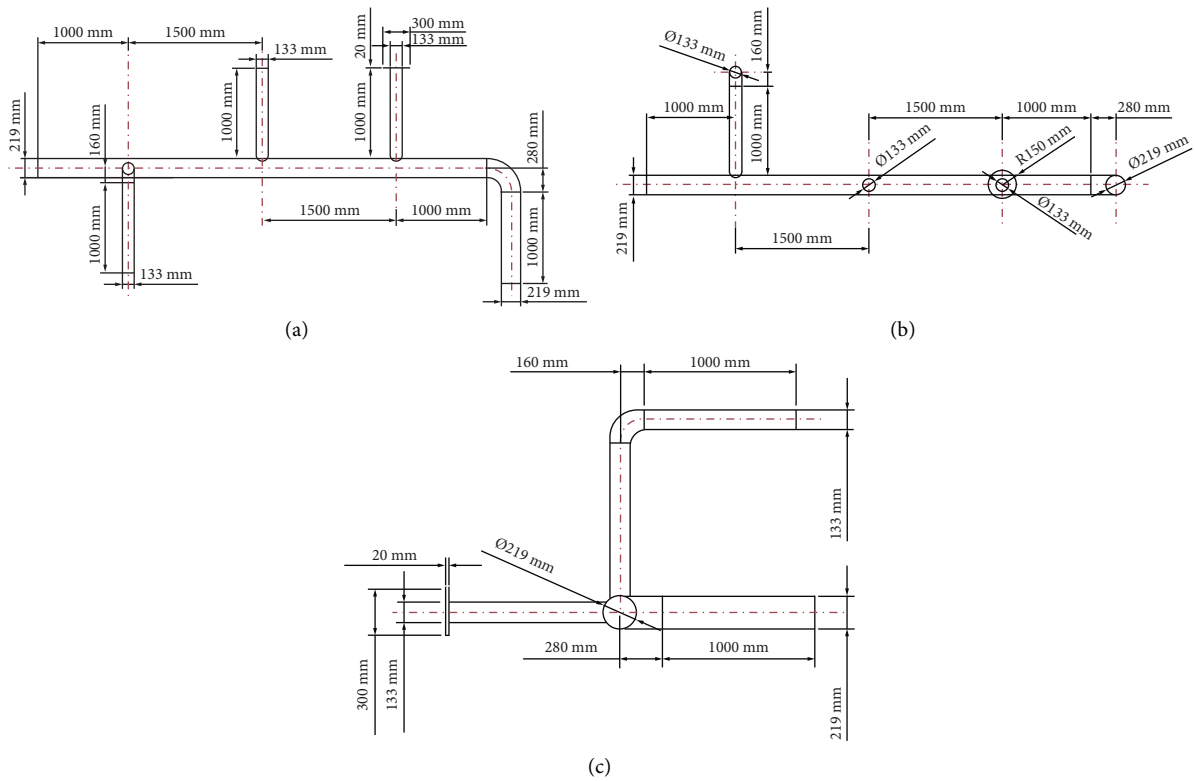

Figure 5: Three views of the real-scale pipeline structure model: (a) top view, (b) front view, and (c) side view.

order to ensure the consistency of the damage degree, the cracks on the main pipe and branch pipe were cut along the circumference of 1/3, as shown in Figures 6(a)–6(c) [21], and the locations were selected at the typical locations of fatigue cracks: (1) the bend of the main pipe, (2) the joint of the mass block pipe and large pipe, and (3) the connection between the vertical bend and the big pipe. For the lossless pipeline models included, a total of 4 test models were obtained, as shown in Table 1. The damage location is represented by the distance from the starting point of the positioning route, as shown in Figure 7 [21].

3.2. Modal Tests and Numerical Simulations of the Pipeline Model

3.2.1. Modal Tests. Some parameters of the vibration signal acquisition equipment (equipment model DH5981) are as follows: The number of channels is 8. The sampling frequency is 2000 Hz. Seven vertically mounted one-way acceleration sensors were used in the test. The installation method was magnetic seat, and the contact surface should be smooth and clean during installation. The installation position of the sensor is selected in the place where vibration is obvious, and these positions are obtained through the finite element simulation and preliminary experiment, as shown in Figure 8 [21]. The vibration characteristic test of the pipeline system model is simulated by force hammer knocking. The average value of each measuring point should be struck 5 times in three directions. When the force hammer strikes the vibration point, the impact speed should be increased appropriately and the combination phenomenon should be avoided to ensure that the force pulse signal peak value is large and that the waveform is smooth, as shown in Figure 9. Each measurement model has 8 channels: 1 force hammer signal channel and 7 acceleration signal channels. Table 2 [21] shows the first ten modal frequencies measured in the modal test of no. 1–4 pipeline systems after modal parameter identification.

3.2.2. Finite Element Numerical Simulation. Four finite element models of pipeline system structures with different damage conditions were established. The model material was no. 20 steel. ANSYS Workbench 2020 R1 was selected for finite element software. The material parameters are shown in Table 3 [21].

Since the test model is simply supported by three ties, in order to more accurately reflect the structural characteristics of the pipeline system model, the displacements in three directions of all nodes on the straight line at the contact point between the pipeline and the ties are restricted; that is, the translational displacement of the pipeline system structure at the boundary is restricted, and the rotational displacement is retained, so as to simulate the simply supported boundary conditions, as shown in Figure 10. Solid tetrahedral elements are used for the finite element model meshes of pipeline systems. The default type of the solid element in ANSYS Workbench is Solid186 (3D20N), and the element size is set to 6 mm.

The finite element model of pipeline systems is modified, and the initial parameters of the finite element model are modified, such as geometry model size, boundary conditions, and material parameters, so that the calculated results of the finite element model can be consistent with the measured values as far as possible [22]. In this paper, the finite element model of the pipeline system structure was modified based on the BP neural network and structural natural frequency. The specific process is shown in Figure 11.

In order to reduce the calculation times of the finite element simulation, the whole model correction process is divided into three steps to gradually make the simulation result close to the measured result. The natural frequency changes in the correction process are shown in Table 4.

First, by comparing the calculation results of the initial finite element model with the experimental results, it is found that there is a large difference between the first- and fourth-order natural frequencies (the two modes are mainly the vibration of the vertical bent pipe and the mass block pipe), while the difference between the other order natural frequencies is small, so the model size is basically reasonable. The error is mainly from the welding process, and the small natural frequency is due to higher stiffness at the welding process. Therefore, the weld of the large pipe and branch pipe is reinforced to increase stiffness here, and only the weld size and the thickness of the mass block are modified to achieve the purpose of revising the finite element model.

In the second step, the size of the three welds was estimated to be between 0 and 60 mm, and the finite element model was established with a step size of 20 mm for calculation. The number of samples was 64. The first ten orders of natural frequencies were taken as the input vector of the network and the size of the three welds as the output vector. After neural network training is completed, the measured natural frequency is input into the neural network, and the dimensions of the three welds are preliminarily obtained as 52 mm, 60 mm, and 1 mm, respectively. The finite element model is reconstructed with the above data, the modal analysis is carried out, and the first ten order natural frequencies of the preliminarily modified model are obtained. Compared with the calculated results of the initial finite element model, the error between the measured frequency and the measured frequency is greatly reduced. However, the fourth-order natural frequency has a large error.

In the third step, based on the weld size determined in the second step, the thickness of the mass block and the weld size of the mass block tube are modified to achieve the purpose of correcting the fourth-order natural frequency of the model. The finite element model was established with the thickness of the mass block being 18–32 mm with a step length of 2 mm and the weld size of the mass block being 0–60 mm with a step length of 10 mm. The number of samples was 48. As in the second step, the first ten orders of natural frequencies are taken as the input vector of the neural network and the thickness of the mass block and the weld size of the mass block tube are taken as the output vector. After training, the output error of the neural network reaches the predetermined target. In the third step, the thickness and weld size after modification are 29 mm and 29 mm. Compared with the frequency

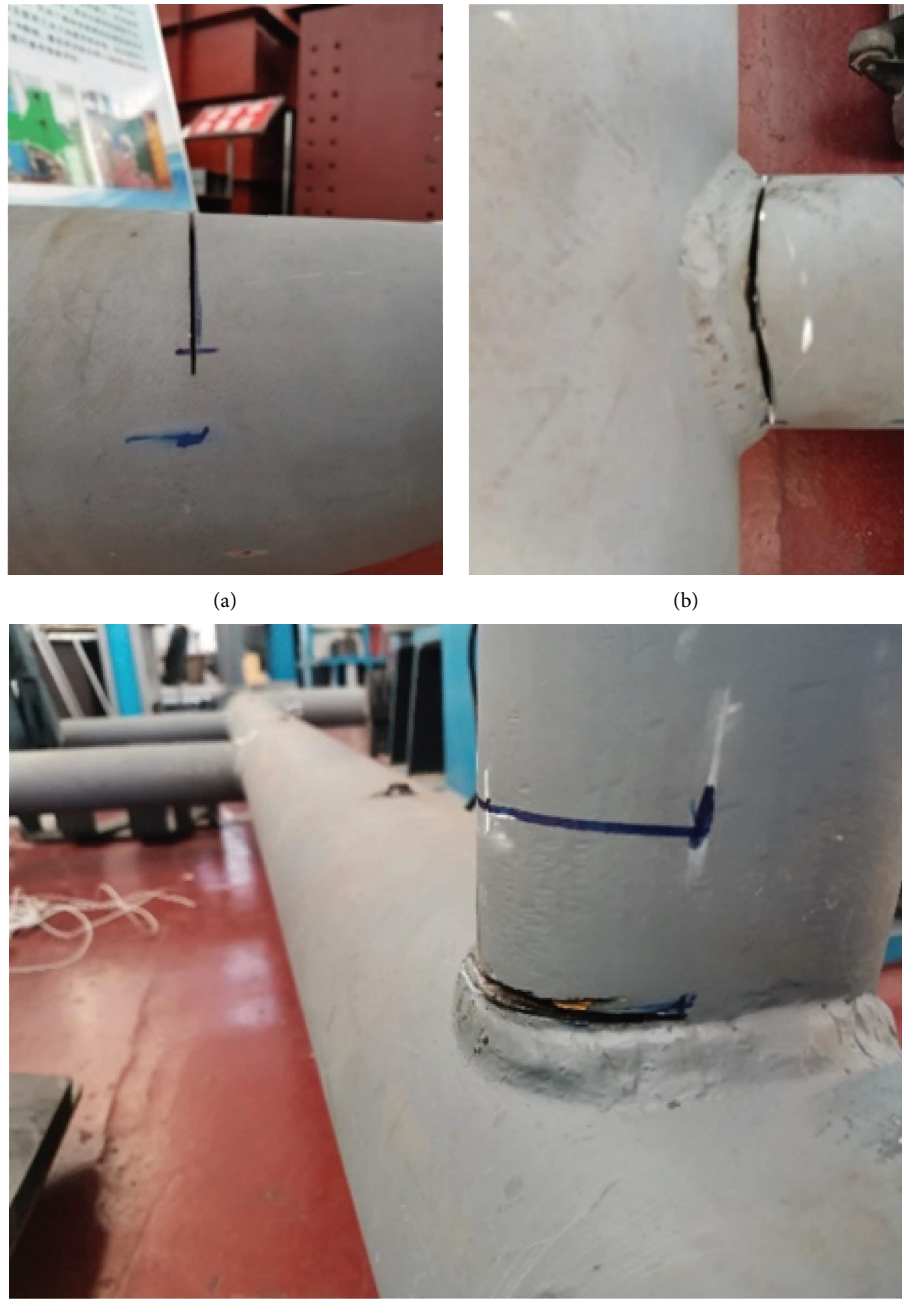

(a) (b) (c)

Figure 6: Pipe model with cracks: (a) large pipe elbow, (b) pipe connection with a mass block, and (c) vertical bent pipe connection.

Table 1: Test models of different crack locations.

Number	Crack location
1	Intact
2	Large pipe elbow, located 1020 mm
3	Pipe connection with a mass block, located 2240 mm
4	Vertical bent pipe connection, located 5240 mm

measured in the test, the error of the simulation results after the size modification is within an acceptable range, so the modification of the finite element model is completed.

After the modification of the finite element model was completed, the modal analysis of no. 1–4 models was carried out by using ANSYS Workbench to obtain the natural frequencies of the pipeline system structure under conditions of nondestructive and different damage locations, and the comparison analysis was made with the modal test results, as shown in Table 5 [21]. The first three modal shapes of the no. 1 model are shown in Figures 12–14. Generally, the lower the natural frequency of the structure, the easier it is to be excited, and the lower order modes are not easy to miss. At the same time, the corresponding amplitude of the lower order natural frequency is larger, and the frequency response function

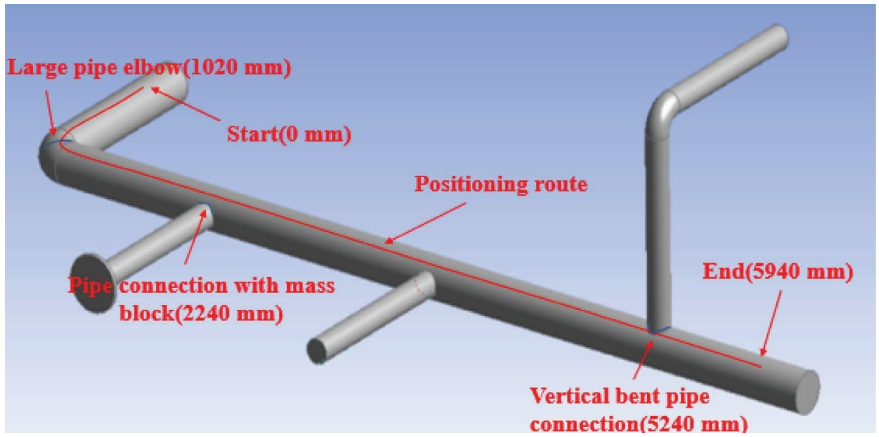

Figure 7: Schematic diagram of crack locations.

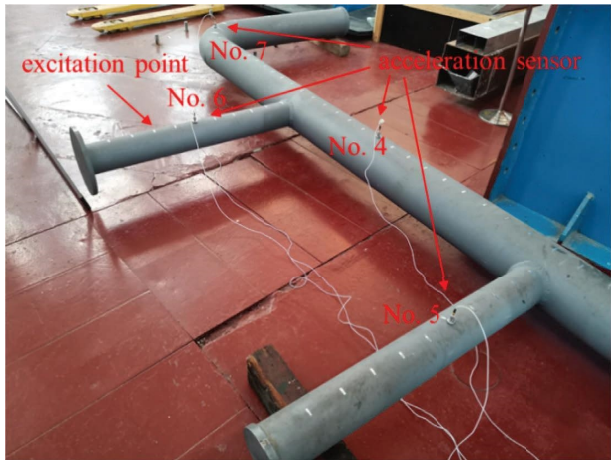

Figure 8: Layout of measuring points.

obtained in the modal test is more accurate, so the lower order natural frequency is also more accurate. In addition, considering the complex structure of the pipeline system, the influence of different damage locations on the first several modes may be similar. Considering the feasibility of damage identification and locations, the first ten natural frequencies of the four pipeline system models were extracted for subsequent research on pipeline fatigue crack identification and locations.

Figure 9: Modal test of pipeline systems under force hammer loading.

Table 2: Measured natural frequencies of the pipeline model (Hz).

Modal order number	Model number			
	No. 1	No. 2	No. 3	No. 4
1	11.694	11.719	11.209	10.668
2	14.089	14.063	13.281	14.063
3	20.411	20.313	20.099	19.531
4	29.892	29.521	27.368	29.363
5	36.045	35.938	31.269	35.938
6	39.111	38.281	36.169	37.632
7	40.715	40.625	40.625	40.625
8	61.765	61.719	61.417	60.536
9	72.592	71.809	71.012	72.026
10	90.633	90.493	90.510	90.308

Table 3: Piping system model material parameters.

Elastic modulus E (GPa)	Poisson ratio (μ)	Density (ρ) (kg/m^3)
206	0.3	7850

After the finite element model modification, there were relative errors between the finite element simulation results of the pipeline system structure and the measured results of the

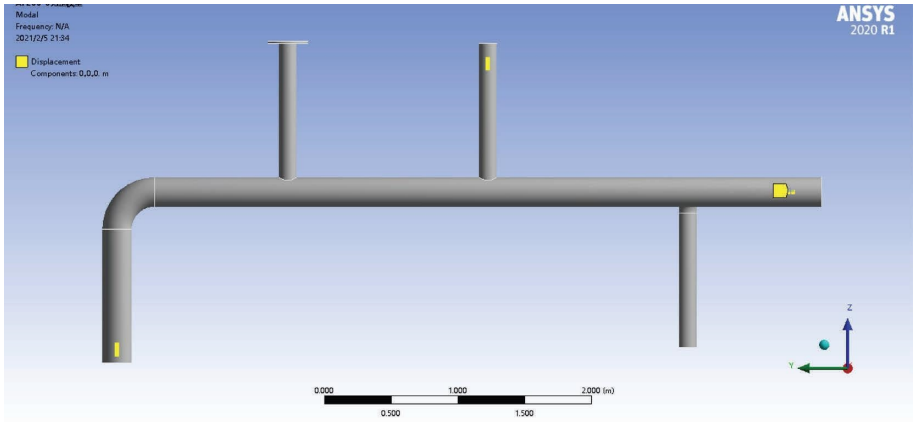

Figure 10: Boundary conditions for the finite element model of pipeline systems.

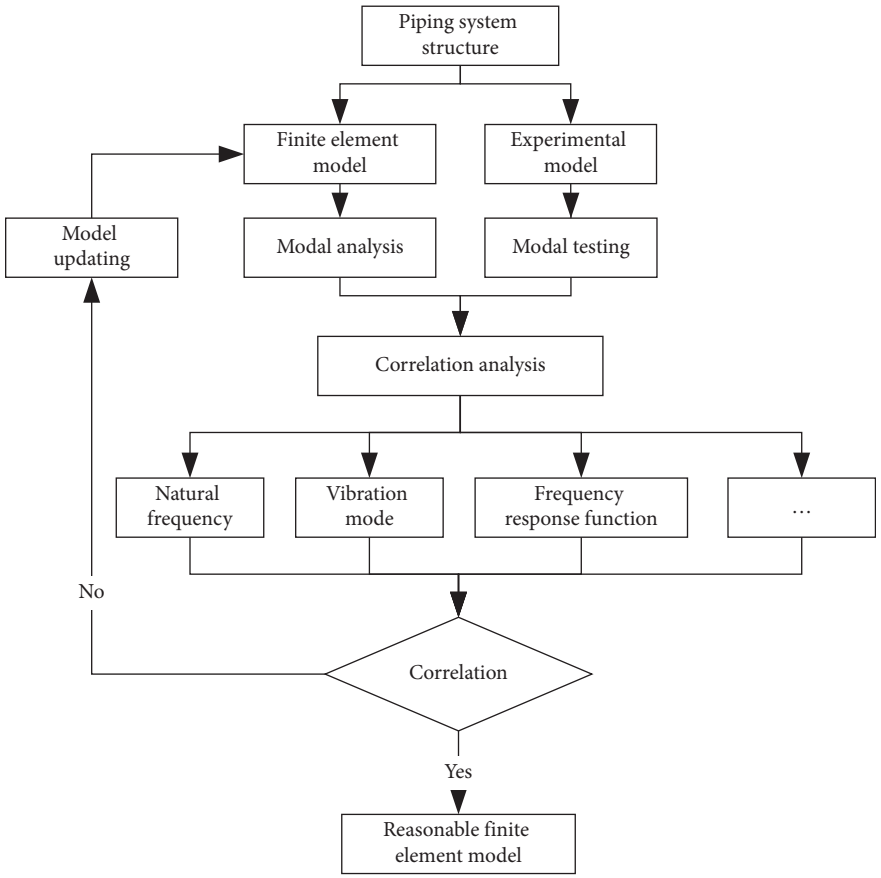

Figure 11: Finite element model revision process.

modal tests. However, the first 10 order normalized frequency change rate (NFCR) results of the finite element simulation calculation and the measured results of the modal test were similar, as shown in Figures 15(a)–15(c) [21].

3.2.3. Creating Damage Conditions. Since neural network damage identification requires a large number of training samples, finite element software ANSYS Workbench is used to create a large number of structural damage conditions for pipeline systems based on the revised finite element model. Damage locations are distributed throughout the entire pipeline structural model, and the form is the same as the test model, which is a circumferential crack with 1/3 of the circumference cut. The crack width was 6 mm, and the damage location was indicated by the method shown in Figure 6. At the same time, artificially added samples are added into the training samples to increase the number of

Table 4: Error comparison of the finite element model modified by the neural network.

Modal degree	Modal testing	Initial finite element model		First-step correction		Second-step correction	
	Measured value (Hz)	Simulation value (Hz)	Relative error (%)	Simulation value (Hz)	Relative error (%)	Simulation value (Hz)	Relative error (%)
1	11.694	9.2847	−20.60	11.787	0.80	11.689	−0.04
2	14.089	13.246	−5.98	14.715	4.44	14.515	3.02
3	20.411	19.044	−6.70	21.724	6.43	21.792	6.77
4	29.892	26.676	−10.76	27.691	−7.36	28.753	−3.81
5	36.045	35.218	−2.29	35.484	−1.56	36.122	0.21
6	39.111	37.017	−5.35	37.921	−3.04	38.341	−1.97
7	40.715	42.536	4.47	42.699	4.87	42.847	5.24
8	61.765	57.739	−6.52	65.384	5.86	65.348	5.80
9	72.592	71.31	−1.77	73.869	1.76	72.275	−0.44
10	90.633	89.325	−1.44	90.319	−0.35	90.183	−0.50
Average	—	—	6.59	—	3.65	—	2.78

training samples of the neural network and enhance the generalization ability of the neural network [23]. The method of adding random white noise is as follows:

$$\gamma_i' = \gamma_i(1 + \varepsilon_i p), \tag{17}$$

where γ_i and γ_i' are the first 10 orders of the standardized NFCR without noise and with added noise, respectively, ε_i is the random number from the standard normal distribution, and P is the percentage of added noise. Finally, the finite element crack conditions of the cracks in the pipeline system are shown in Table 6 [21], and these samples were used as training samples for vibration neural networks.

4. Location Results and Analysis

4.1. Results of Fatigue Crack Locations Based on the BP Neural Network. The BP neural network was used to locate the fatigue cracks of the pipeline system structure, and the first 10 orders of the NFCR under each damage condition were calculated as the feature vector of the damage location. Therefore, the input of the constructed neural network was the first 10 orders of NFCR, and the number of nodes in the input layer was 10. The output was the damage position, and the number of nodes in the output layer was 1. During training, the input and output vectors were normalized to the range of $[-1, 1]$, and the output vectors were reversely normalized during positioning to obtain the fatigue crack location results. The Tansig function was used as the transfer function in the hidden layer, and its expression is

$$y = \frac{2}{\left(1 + e^{-2*\text{net}}\right)} - 1, \tag{18}$$

where y is the neuron output of this layer and net is the neuron input of this layer.

The Purelin function was selected as the output layer, and its expression is

$$y = \text{net}. \tag{19}$$

After repeated network testing, the hidden layer was set to 11, so the constructed BP neural network structure was $10 - 11 - 1$. The initial weight and threshold values of each layer of the BP neural network were randomly set to values within the range of $[-1, 1]$. The reason for this setting was that the BP neural network normalized data to $[-1, 1]$ before training and that the neural network output was also within $[-1, 1]$. Therefore, the weight and threshold values were also of this magnitude. After repeated tests, the learning rate of BP neural network training was set to 0.1 and the learning target was set to 0.001.

After training, the network's ability to locate cracks in the pipeline system was first tested. The finite element method was also used to create damage conditions for the test samples, which were not included in the training samples. The test results are shown in Table 7, where relative error = absolute error/measured pipeline length.

The crack location accuracy near vertical bend pipe-connection (2240mm), mass block pipe connection (5240mm), and pipelinestraddle position is higher than other positions. Compared with the middlesegment, the precision of crack location is poor because there are few-ertraining samples near the simply supported end, and the structural naturalfrequency changes caused by damage near the end are complex.

At the same time, in order to simulate the various errors in the modal test and verify the generalization ability of the BP neural network, 5% noise was added to the test sample to verify the neural network's crack location ability for the pipeline system under the interference of data noise. The location results are shown in Table 8. As shown in Figure 16, the noise had a certain influence on crack location predictions. With the introduction of noise, the crack positioning result error increased slightly. However, overall, the network forecast result was adequate, showing that the proposed method has the ability to resist noise.

Finally, the trained neural network was used to locate the cracks of the damaged pipes from the vibration tests. The results are shown in Table 9. Due to the vibration test errors and noise, the positioning results had large errors, and the relative error was about 10%. However, in general, this method has achieved good results, but there is still room for improvement.

Since the initial weights and thresholds of BP neural network training were randomly set, there was randomness in the final crack location result, this result is the training

Table 5: Numerical simulation results and comparison between the numerical simulation and measured modal results.

Modal order number	Model no. 1		Model no. 2		Model no. 3		Model no. 4	
	Frequency (Hz)	Relative error (%)	Frequency (Hz)	Relative error (%)	Frequency (Hz)	Relative error (%)	Frequency (Hz)	Relative error (%)
1	11.689	−0.04	11.597	−1.04	11.388	1.60	10.559	−1.02
2	14.515	3.02	14.314	1.78	13.385	0.78	14.230	1.19
3	21.792	6.77	21.713	6.89	21.371	6.33	20.785	6.42
4	28.753	−3.81	27.456	−7.00	26.002	−4.99	28.360	−3.42
5	36.122	0.21	36.097	0.44	33.307	6.52	35.986	0.13
6	38.341	−1.97	37.873	−1.07	37.696	4.22	37.696	0.17
7	42.847	5.24	42.846	5.47	42.617	4.90	42.767	5.27
8	65.348	5.80	65.332	5.85	65.328	6.37	64.319	6.25
9	72.275	−0.44	71.442	−0.51	71.080	0.10	72.044	0.02
10	90.183	−0.50	89.383	−1.23	90.177	−0.37	90.068	−0.27
Average		2.78	—	3.13	—	3.62	—	2.42

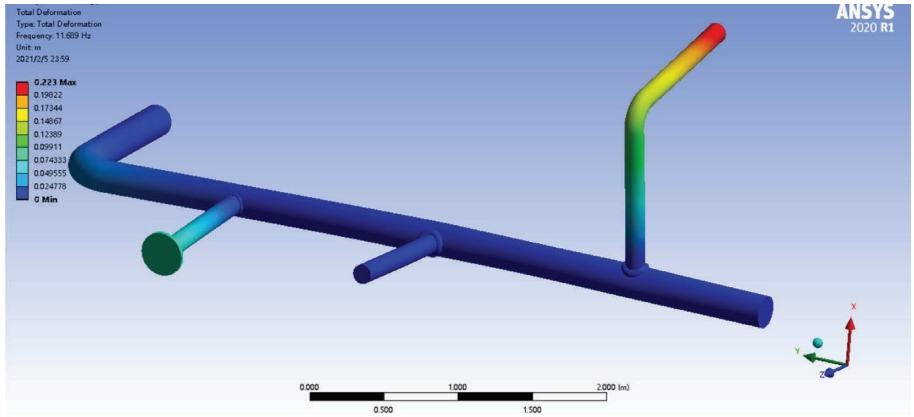

Figure 12: First modal shape of model 1.

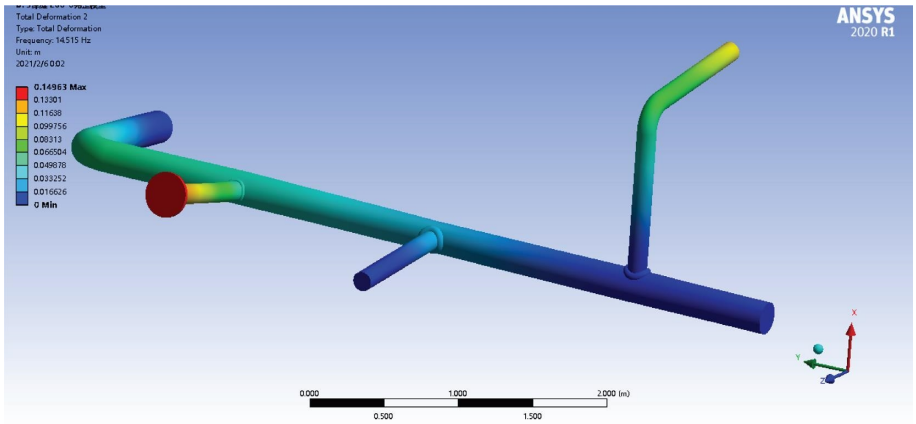

Figure 13: Second modal shape of model 1.

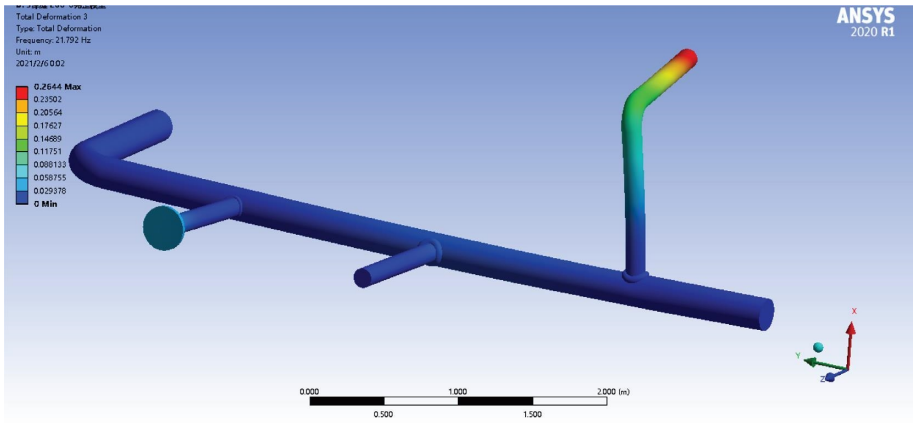

Figure 14: Third modal shape of model 1.

result of BP neural networkwith ideal damage location recognition effect. The differences in the BP neural network training results were due to some of the initial parameter settings causing convergence to local optimal solutions in the training process, which led to the low accuracy of the BP neural network in identifying the damage position of the actual pipeline structure. In order to solve this problem, the GA was adopted to optimize the initial weights and threshold values of BP neural network training for improvement.

4.2. Results of Fatigue Crack Locations Based on the GA-BP Vibration Method. The GA was used to improve the initial weights and thresholds of the BP neural network to optimize

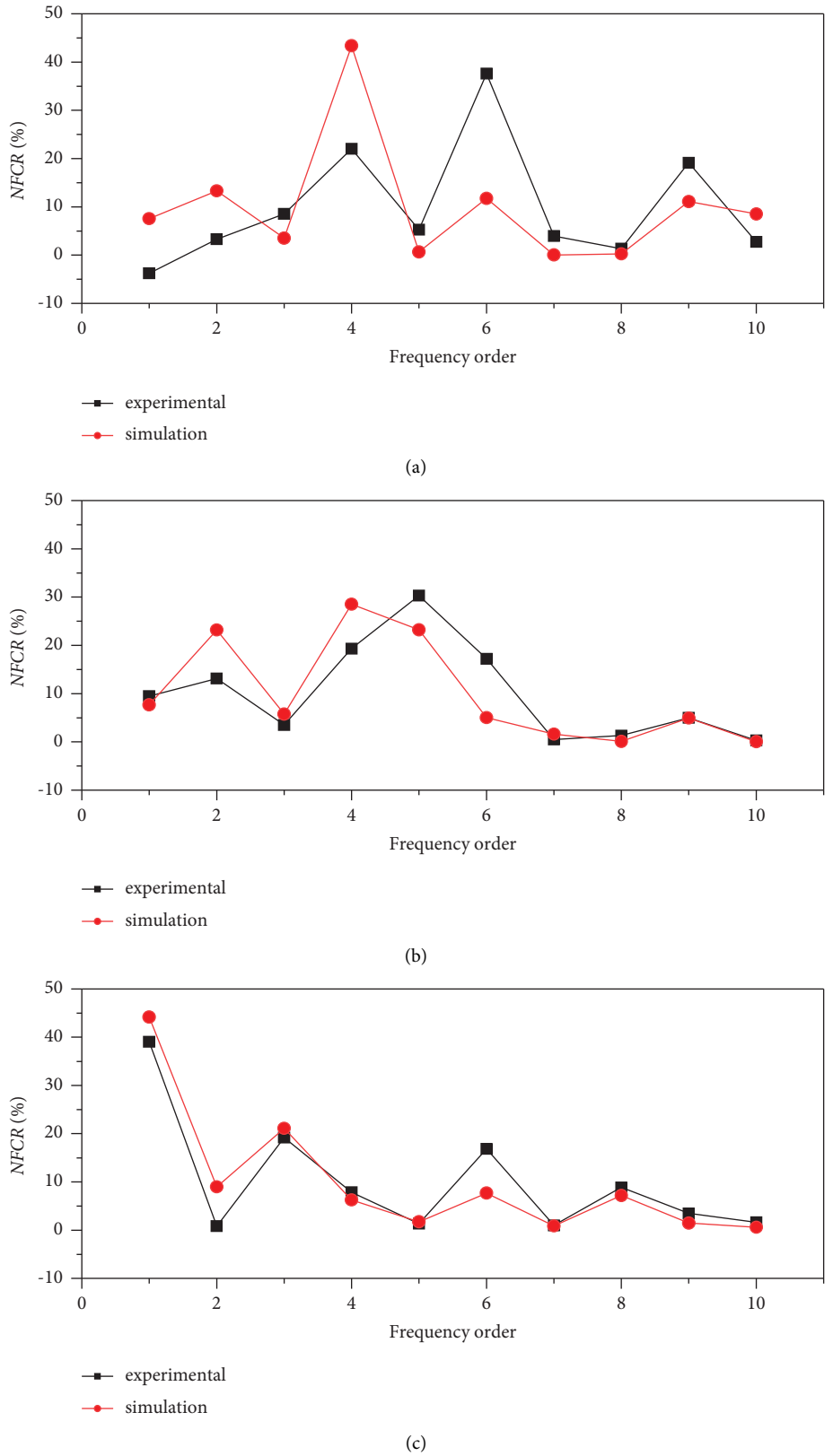

Figure 15: Comparison of the simulation and measured normalized frequency change rates (NFCRs): (a) model 2, (b) model 3, and (c) model 4.

Table 6: Simulation of pipeline crack conditions.

Crack conditions	Noise (%)	Sample size
Main pipe	0	55
Main pipe	5	110
Pipe with mass block	0	10
Pipe with mass block	5	20
Simply supported pipe	0	10
Simply supported pipe	5	20
Vertical bent pipe	0	21
Vertical bent pipe	5	42
Total	—	288

the network training results. A BP neural network with the same structure as that in Section 2 was constructed. The input vector was the first 10 orders of NFCR, the output was the damage position, the BP neural network structure to be optimized was constructed as $10-11-1$, the transfer function of the hidden layer was Tansig, and the transfer function of the output layer was Purelin. The input and output data of the neural network were normalized to the range of $[-1,1]$. During neural network training, the learning rate was set at 0.1 and the learning target was set at 0.001. Parameters to be optimized in the BP neural network were the coding for an individual, the individual lengths of $(10\times 11+11+11\times 1+1)=133$, and the fitness of individuals. The individual contained the initial weights and thresholds of the neural network. During training, the sum of the absolute values of the differences between the predicted and actual crack locations was the fitness value of the individual. The other parameters used by the genetic algorithm are shown in Table 10.

The initial weights and thresholds optimized by the genetic algorithm were passed to the BP neural network for retraining. After training, its ability to locate cracks in the pipeline system was first tested. The damage condition of the test samples was also created by the finite element method, and the results are shown in Table 11. As in Section 4.1, 5% noise was added to the test sample to verify the neural network's crack location ability for the pipeline system under the interference of data noise. The location results are shown in Table 12.

The crack location accuracies near the vertical bend pipe connection (2240 mm), the mass block pipe connection (5240 mm), and the midspan position of the pipe were higher than those in other positions, and the crack location effect near the simple support was poor. With the introduction of noise, the error increased significantly, which was similar to the results of the original BP neural network. This was because the GA only optimized the initial weights and threshold values of the BP neural network and the calculation model used was the same. Under the existing conditions, better positioning results were selected. The results of the crack location in the case with and without data noise are shown in Figure 17.

The trained neural network was used to locate the cracks in the damage conditions of the vibration tests, and the results are shown in Table 13. In general, the positioning method achieved good results, and the average error was reduced by 41.4% compared with the positioning results of the original BP neural network.

4.3. Comparative Analysis of Methods. To compare the training results of the original BP neural network model and those optimized by the GA, commonly used evaluation indices were selected. The output result of the trained neural network should be highly positively correlated with the target output, which can be expressed by the correlation coefficient. The range of the correlation coefficient, R, is within the range of $[-1,1]$, and the closer it is to 1, the better the training effect. The correlation coefficient, R, is defined as

$$R(x,y)=\frac{Cov(x,y)}{\sqrt{\mathrm{Var}[x]\mathrm{Var}[y]}}=\frac{\sum_{i=1}^{n}(x_i-\overline{x})(y_i-\overline{y})}{\sqrt{\sum_{i=1}^{n}(x_i-\overline{x})^2\sum_{i=1}^{n}(y_i-\overline{y})^2}}, \tag{20}$$

where x is the crack location (target output) and y is the predicted location (actual output).

The mean square error was also used to evaluate network performance. A smaller mean square error value indicates that the neural network model has better accuracy in fitting training data. The mean square error (MSE) is defined as

$$\mathrm{MSE}=\frac{1}{n}\sum_{i=1}^{n}(x_i-y_i)^2. \tag{21}$$

For the original BP neural network, $R=0.999131129$ and MSE = 6512.02197, and for the BP neural network optimized based on the genetic algorithm, $R=0.999339613$ and MSE = 6246.65399. Compared with the network before optimization, the training results of the network at this time had smaller errors and better correlations.

The unary linear regression of the predicted results and the actual data were used to reflect the training effect of the neural network. When the output of the neural network is equal to the target, the regression line should coincide with the 45° line. The least squares method was used to carry out unary linear regression for the prediction results of the neural network using the following equations:

$$\begin{aligned} y&=a+bx,\\ a&=\overline{y}-b\overline{x},\\ b&=\frac{\overline{x}\cdot\overline{y}-\overline{xy}}{\overline{x}^2-\overline{x^2}}. \end{aligned} \tag{22}$$

The regression fitting results are shown in Figures 18 and 19. The target value and the output result of the training results of the two models were basically on the same line, but there were fewer outliers in the training results based on the GA-BP method, and the fitting curve was closer to 45°.

To further verify the superiority of the GA-BP neural network, training sample sets were selected at random, and 200 consecutive training processes were conducted using the ordinary BP network and the GA-BP network. The average values of the evaluation indices and the average positioning errors were calculated. The mean values of the evaluation indices of the original BP neural network were $R=0.99872443$ and MSE = 7338.384804, and the average error of the positioning results was 3.37%. The mean values of the evaluation indices of the BP neural network based on

Table 7: Location results of the BP neural network without noise.

Test conditions	Actual position (mm)	Identification results (MM)	Absolute error (mm)	Relative error (%)
1	5790	5514.29	275.71	4.64
2	5240	5186.30	53.70	0.90
3	4790	4765.57	24.43	0.41
4	3740	3689.72	50.28	0.85
5	3690	3440.52	249.48	4.20
6	2990	2992.89	2.89	0.05
7	2240	2249.20	9.20	0.15
8	1790	1804.58	14.58	0.25
9	1690	1738.48	48.48	0.82
10	946.5	926.59	19.91	0.34
11	550	438.78	111.22	1.87
Average	—	—	78.17	1.32

Table 8: BP neural network location results with (%) noise.

Test conditions	Actual position (mm)	Identification results (MM)	Absolute error (mm)	Relative error (%)
1	5790	5436.00	354.00	5.96
2	5240	5207.00	33.00	0.56
3	4790	4793.96	3.96	0.07
4	3740	3690.84	49.16	0.83
5	3690	3405.37	284.63	4.79
6	2990	3047.23	57.23	0.96
7	2240	2246.63	6.63	0.11
8	1790	1894.31	104.31	1.76
9	1690	1716.82	26.82	0.45
10	946.5	965.76	19.26	0.32
11	550	384.30	165.70	2.79
Average	—	—	100.43	1.69

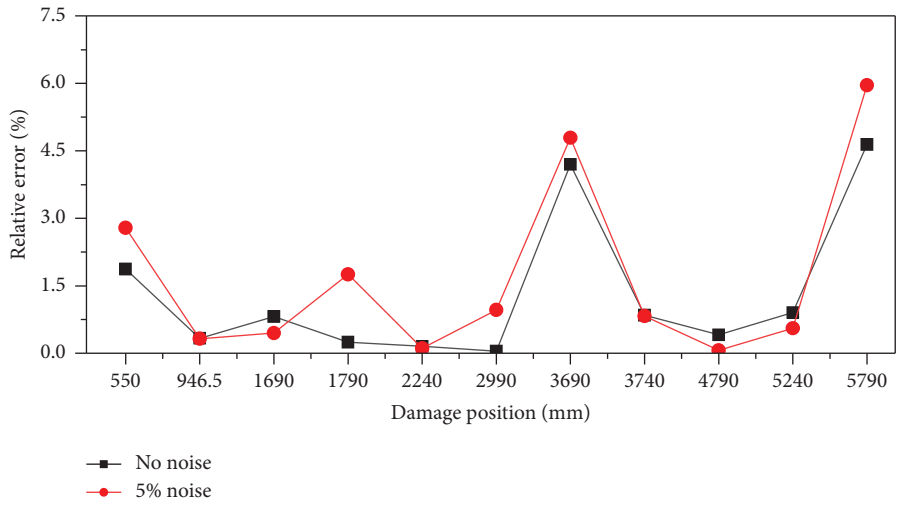

Figure 16: BP neural network localization results for the finite element damage model.

Table 9: Vibration test BP neural network location results.

Model no.	Damage condition	Actual position (mm)	Identification results (MM)	Absolute error (mm)	Relative error (%)
2	At the elbow of the pipe	1020	1308.72	288.72	4.86
3	Mass block pipe connection	2240	2856.29	616.29	10.38
4	Vertical elbow joint	5240	4606.99	633.01	10.66

Table 10: Parameters used in the genetic algorithm.

Parameter	Population size	Chromosome length	Maximal evolutionary algebra	Crossover probability	Mutation probability
Value	40	133	20	0.4	0.2

Table 11: Location results of the noiseless GA-BP neural network.

Test conditions	Actual position (mm)	Identification results (MM)	Absolute error (mm)	Relative error (%)
1	5790	5746.79	43.21	0.73
2	5240	5213.76	26.24	0.44
3	4790	4835.52	45.52	0.77
4	3740	3760.08	20.08	0.34
5	3690	3789.18	99.18	1.67
6	2990	3078.15	88.15	1.48
7	2240	2289.83	49.83	0.84
8	1790	1834.18	44.18	0.74
9	1690	1794.06	104.06	1.75
10	946.5	1052.00	105.50	1.78
11	550	628.03	78.03	1.31
Average	—	—	64.00	1.08

Table 12: GA-BP neural network location results with 5% noise.

Test conditions	Actual position (mm)	Identification results (MM)	Absolute error (mm)	Relative error (%)
1	5790	5531.87	258.13	4.35
2	5240	5218.69	21.31	0.36
3	4790	4827.84	37.84	0.64
4	3740	3770.05	30.05	0.51
5	3690	3779.81	89.81	1.51
6	2990	3094.92	104.92	1.77
7	2240	2286.51	46.51	0.78
8	1790	1937.55	147.55	2.48
9	1690	1805.16	115.16	1.94
10	946.5	1080.22	133.72	2.25
11	550	639.05	89.05	1.50
Average	—	—	97.64	1.64

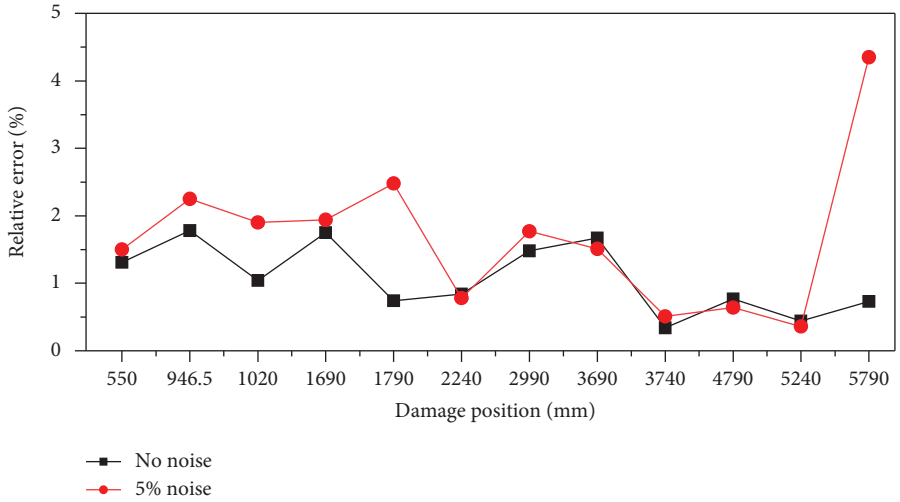

Figure 17: GA-BP neural network localization results of finite element damage conditions.

Table 13: GA BP neural network location results of the vibration test.

Model no.	Damage condition	Actual position (mm)	Identification results (mm)	Absolute error (mm)	Relative error (%)
2	At the elbow of the pipe	1020	1085.86	65.86	1.11
3	Mass block pipe connection	2240	2293.39	53.39	0.90
4	Vertical elbow joint	5240	5084.88	155.12	2.61

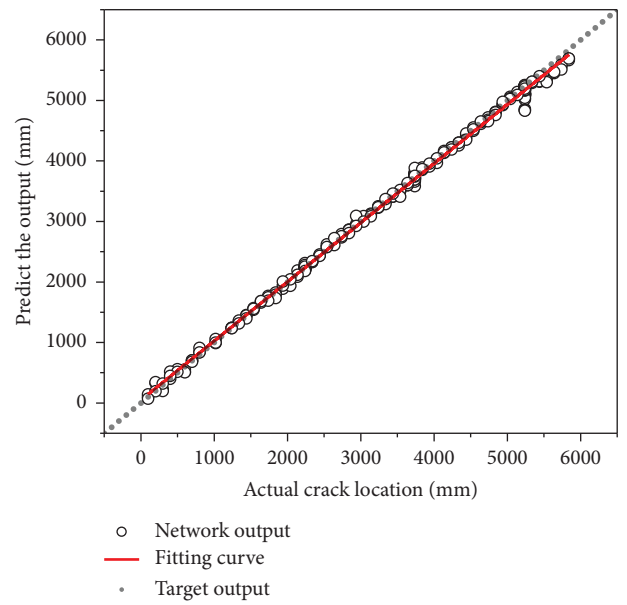

Figure 18: Comparison of the original BP neural network model predictions and actual results.

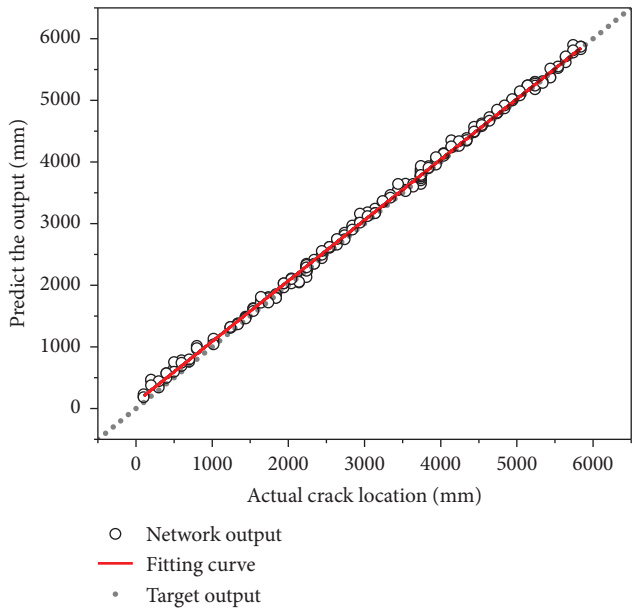

Figure 19: Comparison of the GA-BP neural network model predictions and actual results.

GA optimization were $R = 0.998879998$ and MSE = 6989.501492, and the average error of the positioning results was 2.98%. This suggested that the previous conclusions were not accidental. Compared with the original BP neural network, the BP neural network based on GA optimization had a better training effect and the average positioning error was reduced by 11.6%.

5. Conclusion

In this paper, the damage location of offshore oil and gas pipelines based on vibration tests and the use of a GA-improved BP neural network were studied. The main contributions and conclusions are summarized as follows:

(1) With a real-scale model test for the piping system structure without damage and with different damage locations, the pipeline structure natural frequencies were analyzed. The results were compared with simulation values. Data from experiments of a pipeline system of fixed size were used to validate a finite element simulation model. The size of the simulation model was anastomotic, resulting in a large number of damage condition samples.

(2) A BP neural network was established, and a damage location method based on vibration modal parameters and the BP neural network was used to calculate the normalized natural frequency change ratios under all working conditions. The BP neural network was trained, and damage locations were predicted.

(3) The same damage condition samples were used to train the BP neural network improved by the GA to locate the damaged areas, and neural network training was evaluated by common indices. The results show that, compared with the original BP neural network, the BP neural network based on GA optimization had a better fitting effect and smaller positioning errors. Through a large number of training tests, the contingency of the optimization results was eliminated. The average positioning error is less than 3%, which is reduced by 11.6%, compared to the neural network predictions before optimization.

Data Availability

The data that support the findings of this study are available from the corresponding author upon reasonable request.

Conflicts of Interest

The authors declare that they have no conflicts of interest.

Acknowledgments

This work was supported by the special fund under No. 473 Project (2018) of the Ministry of Industry and Information Technology.

References

[1] O. M. Each and O. M. Each, *Guidelines for the Avoidance of Vibration Induced Fatigue Failure in Process Pipework*, Energy Institute, London, UK, 2008.

[2] T. Contursi, A. Messina, and E. J. Williams, "A multiple-damage location assurance criterion based on natural frequency changes," *Journal of Vibration and Control*, vol. 4, pp. 619–633, 1998.

[3] L. H. Guo, L.-M. Yang, Y.-F. Peng, and Y. Guo, "Fault identification of low-speed hub bearing of crane based on MBMD and BP neural network," *Shock and Vibration*, vol. 2022, Article ID 5005263, 15 pages, 2022.

[4] Z. Rastin, G. Ghodrati Amiri, and E. Darvishan, "Generative adversarial network for damage identification in civil structures," *Shock and Vibration*, vol. 2021, Article ID 3987835, 12 pages, 2021.

[5] P. Cawley and R. D. Adams, "The location of defects in structures from measurements of natural frequencies," *The Journal of Strain Analysis for Engineering Design*, vol. 14, no. 2, pp. 49–57, 1979.

[6] K. He and W. D. Zhu, "Structural damage detection using changes in natural frequencies: theory and applications," *Journal of Physics: Conference Series*, vol. 305, Article ID 012054, 2011.

[7] A. Messina, E. J. Williams, and T. Contursi, "Structural damage detection by a sensitivity and statistical-based method," *Journal of Sound and Vibration*, vol. 216, no. 5, pp. 791–808, 1998.

[8] G. Hearn and R. B. Testa, "Modal analysis for damage detection in structures," *Journal of Structural Engineering*, vol. 117, no. 10, pp. 3042–3063, 1991.

[9] H. Li, H. Tao, and X. Guo, "Damage locating method in stress ducting by frequency change square ratio," *Journal of Dalian University of Technolgy*, vol. 2002, no. 04, pp. 400–403, 2002.

[10] Z. Yang, X. Chen, J. Yu, R. Liu, Z. Liu, and Z. He, "A damage identification approach for plate structures based on frequency measurements," *Nondestructive Testing and Evaluation*, vol. 28, no. 4, pp. 321–341, 2013.

[11] H. Tian, G. Wang, K. Sun, Z. Chen, C. Yan, and D. Cui, "Optimization and design of hammerheads and fenders on scrap metal shredders based on improved genetic algorithm," *Shock and Vibration*, vol. 2021, Article ID 1196299, 13 pages, 2021.

[12] J. Liu, X. Li, X. Zhang, and X. Chen, "Modeling and simulation of energy-regenerative active suspension based on BP neural network PID control," *Shock and Vibration*, vol. 2019, Article ID 4609754, 8 pages, 2019.

[13] Y. Xu, W. Cai, L. Wang, and T. Xie, "Intelligent diagnosis of rolling bearing fault based on improved convolutional neural network and LightGBM," *Shock and Vibration*, vol. 2021, Article ID 1205473, 8 pages, 2021.

[14] M. Li, B. Xu, and J. Kou, "On the combination of genetic algorithms and neural networks," *Systems engineering theory and practice*, vol. 19, no. 2, pp. 65–69, 1999.

[15] H. Ma and G. Yang, "Basic methods and research progress of structural damage detection," *Mechanical progress*, vol. 29, no. 004, pp. 513–527, 1999.

[16] De Rumelhart, G. E. Hinton, and R. J. Williams, "Learning representations by back propagating errors," *Nature*, vol. 323, no. 6088, pp. 533–536, 1986.

[17] P. C. Kaminski, "The approximate location of damage through the analysis of natural frequencies with artificial neural networks," *Proceedings of the Institution of Mechanical Engineers - Part E: Journal of Process Mechanical Engineering*, vol. 209, no. 2, pp. 117–123, 1995.

[18] M. Zhou and S. Sun, *Principle and Application of Genetic Algorithm*, National Defense Industry Press, Arlington, Virginia, 1999.

[19] S. Ding, C. Su, and J. Yu, "An optimizing BP neural network algorithm based on genetic algorithm," *Artificial Intelligence Review*, vol. 36, no. 2, pp. 153–162, 2011.

[20] Gb/T 8163-2008, "State General Administration of the People's Republic of China for Quality Supervision and Inspection and Quarantine," *GB/T 8163-2008 Seamless Steel Tubes for Conveying Fluids*, Standards Press of China, Beijing, China, 2008.

[21] L. Zhou, P. Wang, C. Zhang, X. Qu, C. Gao, and Y. Xie, "Multi-mode fusion BP neural network model with vibration and acoustic emission signals for process pipeline crack location," *Ocean Engineering*, vol. 264, Article ID 112384, 2022.

[22] Q. Du, Y. Cheng, and P. Ren, "FEM model updating of engine block from experimental modal data," *Journal of Machine Design*, vol. 36, no. S2, pp. 14–19, 2019.

[23] M. Sahin and R. A. Shenoi, "Quantification and localisation of damage in beam-like structures by using artificial neural networks with experimental validation," *Engineering Structures*, vol. 25, no. 14, pp. 1785–1802, 2003.